Catalysis Communications 140 (2020) 105999

Contents lists available at ScienceDirect

Catalysis Communications

journal homepage: www.elsevier.com/locate/catcom

Short communication

# Pt mechanical dispersion on non-porous alumina for soot oxidation

C.M. Álvarez-Docio[a,*], R. Portela[b,*], J.J. Reinosa[a], F. Rubio-Marcos[a,c], J.F. Fernández[a]

[a] Instituto de Cerámica y Vidrio, CSIC, C/Kelsen 5, 28049 Madrid, Spain
[b] Instituto de Catálisis y Petroleoquímica, CSIC, Marie Curie 2, 28049 Madrid, Spain
[c] Escuela Politécnica Superior, Universidad Antonio de Nebrija, C/Pirineos, 55, 28040 Madrid, Spain

ARTICLE INFO

*Keywords:*
Soot oxidation
Platinum-based catalyst
Nanodispersion
Ball milling process

ABSTRACT

A sustainable mechanical method to disperse Pt particles on the surface of non-porous α-$Al_2O_3$ microparticles is reported. The hierarchical Pt/α-$Al_2O_3$ catalyst possesses a metal specific surface area one order of magnitude lower than the state-of-the-art γ-$Al_2O_3$ – supported Pt catalysts of similar metal composition and high alumina specific surface area. The relatively large size of the Pt particles seems to favor the catalytic soot oxidation in spite of their relatively low dispersion. As a result, the temperature of half conversion ($T_{50}$ = 440 °C) is lower when compared with conventional Pt/γ-$Al_2O_3$ prepared by the wet impregnation chemical synthesis route.

## 1. Introduction

Metal nanoparticles are dispersed on porous supports by different methods [1] to exploit their extraordinary properties in sensors, medical applications or heterogeneous catalysis. Physical techniques or very sophisticated methods require complicated procedures that are not so easily adapted to the industry. Despite the continuous development of methodologies that allow a precise control of catalyst's architecture, the most common synthesis procedures for dispersed metallic catalysts are still the wet chemical methods, such as the incipient wetness impregnation [2]. Though the practical execution is apparently simple, the fundamental phenomena underlying impregnation and drying are complex [3]. Typically, metal precursor-support interactions are limited, thereby permitting the active phase redistribution over the support surface during drying. Also, the impregnation and drying steps involve mass and heat transfer processes [4] that often do not reach equilibrium, resulting in non-uniform concentration profiles in the solid [5]. Moreover, the presence of the active phase(s) inside the small pores may complicate their accessibility for reactant gases, and especially for solid reactants, leading to mass and/or heat transfer limitations. These reasons justify the interest in finding alternative efficient and simple nanodispersion strategies.

The mechano-chemical synthesis of inorganic materials has been used for years, but its application in the context of heterogeneous catalysis is scarce, and it has been largely limited to the processing of support [6]. The use of mechanical methods for the synthesis of catalysts may improve the atomic efficiency, while reducing the use of solvents and the number of synthetic steps, thus contributing to the catalytic process sustainability. Moreover, there is growing evidence of the advantages of mechano-chemical methods for doped metal oxides and mixed metal oxides synthesis/activation, not only in terms of cost and sustainability, but also of catalytic properties, due to the creation of defects, particle size reduction, or promotion of interactions between components [7,8].

Pt/$Al_2O_3$ is a catalyst for many reactions, and the most widely used catalyst for soot oxidation so far because of its high activity and durability [9,10]. Soot oxidation is a demanding reaction, where the contact between gaseous oxidants, soot and active sites is a key parameter, and the price of the catalyst, as in all environmental processes, needs to be reduced. We have recently demonstrated the mechanical activation by low-energy ball milling of a non-porous $CoAl_2O_4$ spinel to catalyze the oxidation of soot efficiently [11]. A similar procedure was applied here to obtain a Pt/α-$Al_2O_3$ catalyst by mechanical dispersion of Pt metal, which was tested for soot oxidation with NO/$O_2$ as benchmark reaction. The proposed methodology is based on a dry nanodispersion method consisting on milling metal oxides with dissimilar composition and size to produce hierarchical nanoparticle-microparticle oxide systems, in which unusual properties arise [12,13].

The objective is to adapt the ball milling method to obtain hierarchal catalysts of nanodispersed noble-metal particles on non-porous micrometric supports with superior reactivity, thereby reducing the catalyst volume, and thus the required reactor size. This efficient synthetic procedure provides a feasible, low-waste, safe-by-design, mass production solution for practical applications that could be used for the deposition of efficient catalytic coatings on the walls of catalytic microreactors [14]. In addition, the method should be easily adapted to

* Corresponding authors.
*E-mail addresses:* carmenma.docio@icv.csic.es (C.M. Álvarez-Docio), raquel.portela@csic.es (R. Portela).

https://doi.org/10.1016/j.catcom.2020.105999
Received 16 October 2019; Received in revised form 23 March 2020; Accepted 27 March 2020
Available online 28 March 2020
1566-7367/ 

employ more advanced supports such as alumina promoted with ceria, which has been reported to largely enhance the rate of soot oxidation by the participation of mobile lattice oxygen of ceria [15,16].

## 2. Experimental

### 2.1. Catalysts preparation

A Pt/α-$Al_2O_3$ catalyst with dispersed Pt particles was prepared by low-energy wet milling incorporating the appropriate amount of $PtO_2$ nanoparticles (Aldrich) into α-$Al_2O_3$ micrometric support (Vicar S.A., $S_{BET}$ = 13.8 $m^2$/g, $V_p$ = 0.04 $cm^3$/g). The α-$Al_2O_3$ microparticles used as support of Pt had a purity > 99.5% and an average particle size of ~6.0 μm. The $PtO_2$ nanoparticles had a high purity (> 99.9%) and average particle size of ~20 nm and formed agglomerates larger than 20 μm. The as-received $PtO_2$ powder was first introduced in a 60 $cm^3$ nylon container and ball-milled in 20 $cm^3$ ethanol during 1 h at 500 rpm to break the agglomerates and facilitate the dispersion. Then, the α-$Al_2O_3$ microparticles were added and the mixture was homogenized by the same ball-milling procedure for 10 min. The whole ball-milling process was assisted by $Al_2O_3$ balls (1 mm in diameter), with a ratio of mass of grinding balls to mass of powder equal to 1:1 (w/w). For comparison, Pt/α-$Al_2O_3$ and Pt/γ-$Al_2O_3$ catalysts were prepared by the incipient wetness impregnation technique using the same α-$Al_2O_3$as in the mechanical method. The γ-$Al_2O_3$was provided by Girdler Südchemie ($S_{BET}$ = 160 $m^2$/g, $V_p$ = 0.32 $cm^3$/g). The mean pore size of the α-$Al_2O_3$ and γ-$Al_2O_3$ were 3.2 and 10 nm, respectively. The corresponding alumina support was impregnated with 1 wt% Pt using an aqueous solution of tetraammineplatinum (II) nitrate $[Pt(NH_3)_4](NO_3)_2$ (Johnson Matthey, 2.648 wt% solution). Finally, all the samples were thermally treated at 550 °C under 10 vol% $H_2$ in $N_2$ gas atmosphere with a heating rate of 20 °C/min in order to reduce the Pt metal oxide to the Pt metallic phase.

### 2.2. Catalysts characterization

The crystalline phases of supported Pt catalysts were characterized by powder X-ray diffraction (XRD, D8, Bruker) using a Lynx Eye detector and Cu $K\alpha_1$ radiation. The morphology of the catalysts (secondary particles/agglomerates) was evaluated by secondary electron images of field emission scanning electron microscopy (FE-SEM, Hitachi S-4700). The particle size distribution was obtained by processing the FE-SEM micrographs with Leica Qwin Image software. A statistical study was performed with values from more than 150 measured particles. The Brunauer-Emmett-Teller (BET) equation was used to determine the specific surface areas of the catalysts based on $N_2$ adsorption-desorption data obtained in a Micrometrics ASAP2020 textural analyzer. The surface composition was determined using an X-ray Photoelectron Spectrometer (XPS, K-alpha, Thermo Scientific), equipped with a monochromated Al Kα (1486.6 eV) source running at a voltage of 12 KV. Pass energy of 200 eV was used for survey scans, while for high-resolution scans the pass energy was 40 eV. Finally, for charge correction a 1 point scale with the C 1 s peak shifted to 285 eV was used. UV–Vis diffuse reflectance spectra of the samples were recorded using a Perkin Elmer Lambda 650 UV–Vis spectrophotometer with an integrated sphere attachment. The Kubelka-Munk function was used to transform the results from diffuse reflectance to absorbance. The points were measured every 2 nm each second.

### 2.3. Catalytic tests

The catalytic activity for soot oxidation was evaluated by temperature-programmed reaction in a fixed-bed tubular reactor system with a ramp from 25 to 750 °C at 5 °C/min. The soot particles were obtained by burning commercial diesel fuel (British Petroleum, Spain) in a glass vessel. Catalyst (100 mg, 0.125–0.250 μm) and soot (10 mg, similar particle size as of catalyst) were carefully mixed to simulate loose-contact mode, diluted with 1 g of SiC to minimize pressure drop and favor heat transfer, and placed in the middle part of the reactor (ϕ = 4 mm; bed length = 70 mm). The feed gas stream comprised of 2500 ppm $NO_x$ ($NO/NO_2$~4), 10% $O_2$ and $N_2$ as balance gas; the total gas flow was 300 mL/min (GHSV ~150,000 $h^{-1}$) (see Table S1 and related text). The fixed-bed reactor outlet composition was analyzed with a Thermo Nicolet FT-IR spectrometer. Blank experiments were also conducted without catalyst in order to analyze the non-catalytic soot oxidation, and without soot in order to analyze the NO to $NO_2$ conversion ability of the catalysts.

The catalytic performance of the ball-milled Pt/α-$Al_2O_3$ catalyst for soot oxidation with only $O_2$ was evaluated by simultaneous thermogravimetric and differential thermal analysis (STA 6000, PerkinElmer) connected to a Fourier transform infrared (FTIR) spectrometer equipped with a gas cell (Frontier, PerkinElmer). About 25 mg of catalyst in powder form was placed in an alumina crucible and subjected to a temperature ramp of 10 °C/min up to 950 °C in air atmosphere.

The soot oxidation catalytic activity was quantified in terms of $T_{10}$, $T_{50}$ and $T_{90}$, the temperatures for 10, 50 and 90% soot conversion, respectively. Soot conversion was estimated as the fraction of the total carbon reacted to produce CO and/or $CO_2$ by the integration of their concentration profiles. The selectivity to $CO_2$ ($S_{CO2}$) was estimated as the $CO_2$ outlet concentration divided by the sum of the $CO_2$ and CO outlet concentrations. The generation of $NO_2$ is expressed as the $NO_2$ fraction of the total amount of $NO_x$ ($NO + NO_2$) fed in the reactor.

## 3. Results and discussion

### 3.1. Textural and structural characterization

Fig. 1a presents the powder XRD patterns obtained for the as-received and ball-milled $PtO_2$ raw material and the Pt/α-$Al_2O_3$sampleprepared by the mechanical dispersion and after treatment in $H_2$ at 500 °C. The diffraction peaks of ball-milled $PtO_2$ are readily indexed to metallic Pt phase, indicating that during the first step of the ball-milling procedure, $PtO_2$ was reduced into the highly stable metallic Pt phase. The energy released during the ball-milling in the presence of ethanol, already known as reducer for Pt oxide even at room temperature [17], was high enough to cause reduction to Pt, and, probably, oxidation of ethanol [18–20]. The ball-milled reduced Pt/α-$Al_2O_3$ catalyst evidences sharp peaks clearly assigned to the α-alumina support, and very low-intensity broad peaks related to the metallic Pt phase; small Pt amount and size of the crystalline domains. Fig. S1a shows the magnification of the 2θ ranges marked in Fig. 1a with blue and pink rectangles, where the presence of metallic Pt and also of the $PtO_2$ phase can be guessed. To verify the chemical state of the Pt active component on the surface of the reduced catalyst, the sample was characterized by XPS (see Fig. S1b). The deconvolution of the spectrum in the Pt 4d region into the individual components revealed the presence of two chemical environments for Pt, attributed to $Pt^0$ and $Pt^{2+}$. Hence, in spite of the already reduced state of Pt when the support microparticles are added to the ball mill, according to the XRD results, and of the high-temperature reduction after treatment performed, some $PtO_2$ is present on the surface. The platinum oxide might have been formed by re-oxidation due to air exposure after the reduction treatment. However, $H_2$-reduced Pt is not so easy to be re-oxidized [21], in particular, relatively large Pt particles [22], where the influence of exposure to air is strongly dependent on the catalyst support chemical composition [23], for example with easily reducible supports, like ceria [24] (alpha-alumina microparticles are not reducible). The metal re-oxidation could also have been induced by the formation of Pt-O-Al interactions with α-$Al_2O_3$, despite the relatively large size of Pt particles. Defects formation on α-alumina surfaces increases their interaction with metals [25], so the intense forces generated in the ball-milling process in the presence of ethanol could have promoted the metal-support interactions, and

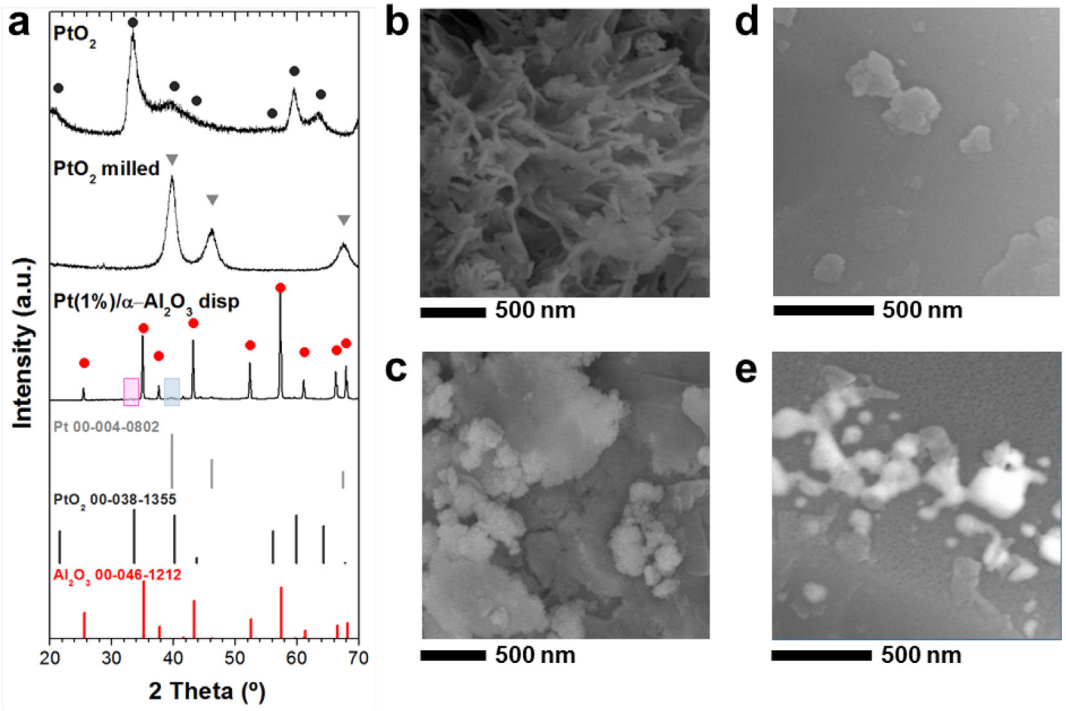


**Fig. 1.** (a) XRD patterns of the as-received and ball-milled $PtO_2$ raw material, the milled Pt(1%)/α-$Al_2O_3$ catalyst and JCPD standards for Pt, $PtO_2$ and α-$Al_2O_3$. Magnifications in the ranges marked with blue and pink rectangles are shown in Fig. S1a. On the right, high-resolution FE-SEM images of $PtO_2$ nanoparticles: as-received (b) and ball-milled (c) and of Pt/α-$Al_2O_3$ samples: milled (d) and impregnated (e). Ball-milled Pt-based catalyst onα-$Al_2O_3$ microparticles shows the alumina surface covered by Pt-based particles (d), and impregnated Pt/α-$Al_2O_3$shows surface exsolution of Pt-based particles (e). Lower magnification micrographs and micrographs of the impregnated Pt/γ-$Al_2O_3$ sample are shown in the Supplementary Information.

these would be maintained or even increased after the reduction process in $H_2/N_2$ atmosphere at the relatively high temperature of 550 °C.

The morphology of the as-received and ball-milled $PtO_2$ raw material and of the Pt/α-$Al_2O_3$ catalysts prepared by ball milling and the incipient wetness impregnation was investigated by FE-SEM and high-resolution (HR) images are shown in Fig. 1b-e. Specifically, the $PtO_2$powder morphology at local scale consisted mainly of flake-like particles of 100 to 200 nm in size and ~20 nm in thickness that formed the house-of-card structure observed in Fig. 1b, which is related to their electrostatic charge. The ball milling process of the $PtO_2$ precursor reduced not only the oxidation state of Pt, but also the size of the agglomerates at the microscale (see Fig. S1c, d), while at the nanoscale, the flake-like morphology is substituted by agglomerates (Fig. 1c).

According with FE-SEM images (Fig. 1e and Fig. S2f) and EDX mapping (Fig. S2g), in the impregnated Pt/α-$Al_2O_3$ sample, the platinum particles exsoluted into interconnected and micrometer-sized agglomerates located in certain areas on the surface of the alumina microparticles. Meanwhile, in the ball-milled Pt/α-$Al_2O_3$ sample, the Pt particles seem to be relatively better dispersed on the surface of the α-$Al_2O_3$, and the morphology resembles the lamellar shape of the Pt-precursor (see Fig. S2b for FE-SEM and Fig. S2c for EDX). The particle size distribution is quite similar in both samples (Fig. S2a, e) with an average diameter of 137 ± 84 nm (impregnation) and 178 ± 56 nm (mechanical dispersion), and a very low number of particles larger than 1 μm. Therefore, from a microscopic perspective, it is difficult to clearly estimate the dispersion and differences between both processes (impregnation and mechanical dispersion), and $H_2$-chemisorption is also not informative in this particle size range.

A better dispersion is related to enhanced metal-support interactions [26], and UV–Vis absorbance can be a good technique to compare the degree of dispersion in similar materials, as a finger-print of the Pt electronic interactions [27]. Fig. S3 shows the low absorbance of the impregnated Pt/α-$Al_2O_3$ catalyst compared to the milled sample, indicative of a more effective dispersion of the latter.

### 3.2. Catalytic soot oxidation activity

The results of soot oxidation under $NO_2/O_2$with and without the presence of Pt/$Al_2O_3$ catalysts are shown in Fig. 2a-c. For comparison of the catalytic behavior, Table 1 compiles the temperatures required to achieve 10, 50 and 90% soot conversion and the selectivity to $CO_2$ (calculated by integration of the concentration profiles shown in Fig. 2b) and also the values for representative catalysts reported in the literature. It must be remarked that some of the operating conditions differ in the bibliographic data, so only a tentative, comparison is attempted here. Therefore, as reference, the results of a Pt/γ-$Al_2O_3$ sample prepared by the incipient wetness impregnation and tested at the same conditions are included; SEM micrographs showing the mesoporous structure of this sample are included in Fig. S1e, f. Table 1 also summarizes the specific surface area and Pt particle size reported for the different Pt/$Al_2O_3$ catalysts.

In the non-catalytic soot oxidation, the latter is not consumed completely until the reaction temperature exceeded 600 °C, and 33% of the soot was only partially oxidized to CO. With the synthetized Pt/$Al_2O_3$ catalysts, the temperature required is lower and the selectivity to $CO_2$ is complete. The temperature of 10%, 50%, and 90% soot conversion decreased by 76 °C, 129 °C and 146 °C, respectively, with the ball-milled hierarchical Pt/α-$Al_2O_3$ catalyst, which shows soot conversion temperatures significantly better that the impregnated Pt/α-$Al_2O_3$ sample, and similar to the impregnated Pt/γ-$Al_2O_3$ sample prepared as reference sample. Moreover, the $T_{50}$ of the mechanically dispersed catalyst is lower than that of the most active Pt/γ-$Al_2O_3$catalysts obtained by impregnation and reported in the literature, and 76 °C lower than that of the commercial Pt/γ-$Al_2O_3$sample tested. The evolution of the catalytic oxidation of NO to $NO_2$ by the mechanically dispersed Pt/α-$Al_2O_3$ catalyst with and without soot is given in Fig. 2c. The high NO oxidation capacity of this catalyst, higher than that of the other synthetized samples (results not shown), explains the high soot oxidation activity obtained, because $NO_2$ is a much stronger oxidizing

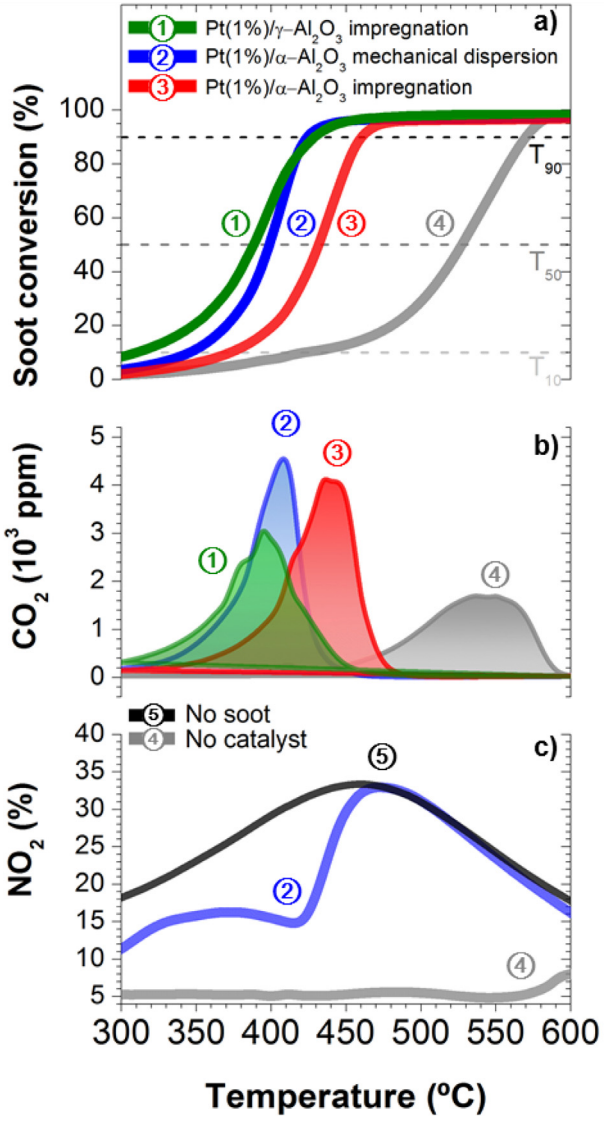


**Fig. 2.** Soot oxidation performance results with the Pt catalysts prepared by impregnation of γ-alumina (green curve, 1), by wet milling with α-alumina (blue curve, 2) or by impregnation of γ-alumina (red curve, 3) and soot combustion results without catalysts (grey curve, 4): (a) Soot conversion vs T profiles, (b) $CO_2$ formation vs T profiles, and (c) $NO_2$ to total $NO_x$ fraction vs T profiles. Reaction conditions: 100 mg catalyst +10 mg soot; dilution with SiC; loose contact; 2500 ppm NO +10 vol% $O_2$ + $N_2$ (300 mL/min). The black curve with number 5 in panel (c) is a similar experiment to curve 2, with the ball-milled Pt/α-$Al_2O_3$ catalyst but without soot (blank experiment). (For interpretation of the references to colour in this figure legend, the reader is referred to the web version of this article.)

agent than NO and $O_2$. In fact, the oxidation profiles obtained in a NO-free gas atmosphere, illustrated in Fig. S4, confirm that the absence of the $NO_2$-assisted mechanism shifts the temperatures of soot oxidation toward values similar to the non-catalytic oxidation.

In the hierarchical catalyst based on alpha-alumina, the available specific surface area and pore volume are almost one order of magnitude lower than in the other catalysts for comparison based on the mesoporous gamma-alumina. Consequently, the Pt in such a small area is comparatively less dispersed and should be located outside the pores of the support. In the case of Pt/α-$Al_2O_3$ prepared by impregnation, the agglomeration of Pt-based particles is detrimental for the activity. Meanwhile, the lower size of the Pt particles obtained by impregnation of gamma-alumina, non-detectable in the FE-SEM micrograph of γ-$Al_2O_3$ (Fig. S1f), must be related to their location inside the alumina mesopores. Hence, the use of gamma-alumina increases the metal dispersion and the catalytic activity, and the explanation for the good performance in soot oxidation of the ball-milled Pt/α-$Al_2O_3$ catalyst must be then related to the better accessibility of reactants and dissipation of heat from the exothermal reaction due to the external location of the mechanically dispersed active sites. Another factor that may contribute to the good activity of the ball-milled Pt/α-$Al_2O_3$ is the enhancement of NO dissociation and subsequent oxidation in the larger but relatively dispersed Pt particles. Noble metal particles within the nanometer range, generally below 5 nm, are usually more active than larger particles in oxidation reactions [31]. For instance, the best CO oxidation results with a Pt/$Al_2O_3$ catalyst were obtained in the range of 1–10 nm with particles of 2–3 nm [32]. By contrast, the opposite dependence applies for the NO oxidation [33,34]. Larger Pt clusters bind oxygen more weakly, and thus have higher vacancy concentrations and facile oxygen desorption [35]. In summary, the three synthetic routes of alumina supported Pt catalysts used in this work are schematically compared in Fig. 3.

As catalyst stability is critical for practical applications, to evaluate the reproducibility of the catalyst performance the used sample was recycled for a second soot oxidation test under identical reaction conditions by recharging the soot load. The ball-milled Pt/$Al_2O_3$ catalyst essentially maintains its initial activity. The slight increase of the $T_{50}$ value in the second soot oxidation cycle, of 26 °C, could be mainly attributed to the methodology employed to reload the reactor and the subsequent loss of some of the catalyst mass, although some sintering or defects reconstruction cannot be discarded. Small increases of 10 and 40 °C were also observed with the impregnated reference samples based on alpha and gamma alumina, respectively, which might be related to the lower stability of the latter phase at the high temperatures achieved in the reactor, ca. 750 °C.

Finally, the present work may lay the grounds for the integration of the mechanical nanodispersion method in microreactor technology. We have demonstrated that efficient platinum catalysts can be obtained using non-porous supports, of higher density than gamma-alumina, and thus more active per unit volume. Hence, with the application of the hierarchical catalyst concept, microchannel walls might be effectively covered with active material by direct immersion in wet-milled slurries. The concept here reported would represent a step ahead toward

**Table 1**
Comparison of diesel soot oxidation catalysts prepared by different methods but with the same chemical composition (1 wt% Pt supported on alumina), tested in realistic laboratory conditions ("loose" soot-catalyst contact and $NO_x$ + $O_2$ gas mixture).

| Catalyst | $S_{BET}$ ($m^2$/g) | Pt particle size (nm) | $T_{10}$ (°C) | $T_{50}$ (°C) | $T_{90}$ (°C) | $S_{CO2}$ (%) | $T_{50}$-reused (°C) | Catalyst preparation | Ref. |
|---|---|---|---|---|---|---|---|---|---|
| No catalyst | | | 421 | 527 | 570 | 67 | | | This work |
| Pt/α-$Al_2O_3$ | 15.0 | 178 ± 56 | 345 | 398 | 424 | 100 | 424 | Mechanical dispersion/$PtO_2$ | This work |
| Pt/α-$Al_2O_3$ | 14.0 | 137 ± 84 | 373 | 434 | 465 | 97 | 444 | Impregnation/$[Pt(NH_3)_4](NO_3)_2$ | This work |
| Pt/γ-$Al_2O_3$ | 160 | – | 313 | 389 | 429 | 99 | 429 | Impregnation/$[Pt(NH_3)_4](NO_3)_2$ | This work |
| Pt/γ-$Al_2O_3$ | 138 | 1.8 | 405 | 485 | 490 | > 98 | – | Impregnation/$Pt(NO_3)_2$ | [28] |
| Pt/γ-$Al_2O_3$ | 137 | 7.2 | 360 | 446 | 500 | – | – | Impregnation/Polyol process | [29] |
| Pt/γ-$Al_2O_3$ | 160 | 3.2 | 370 | 474 | 550 | 100 | – | Sigma-Aldrich | [30] |

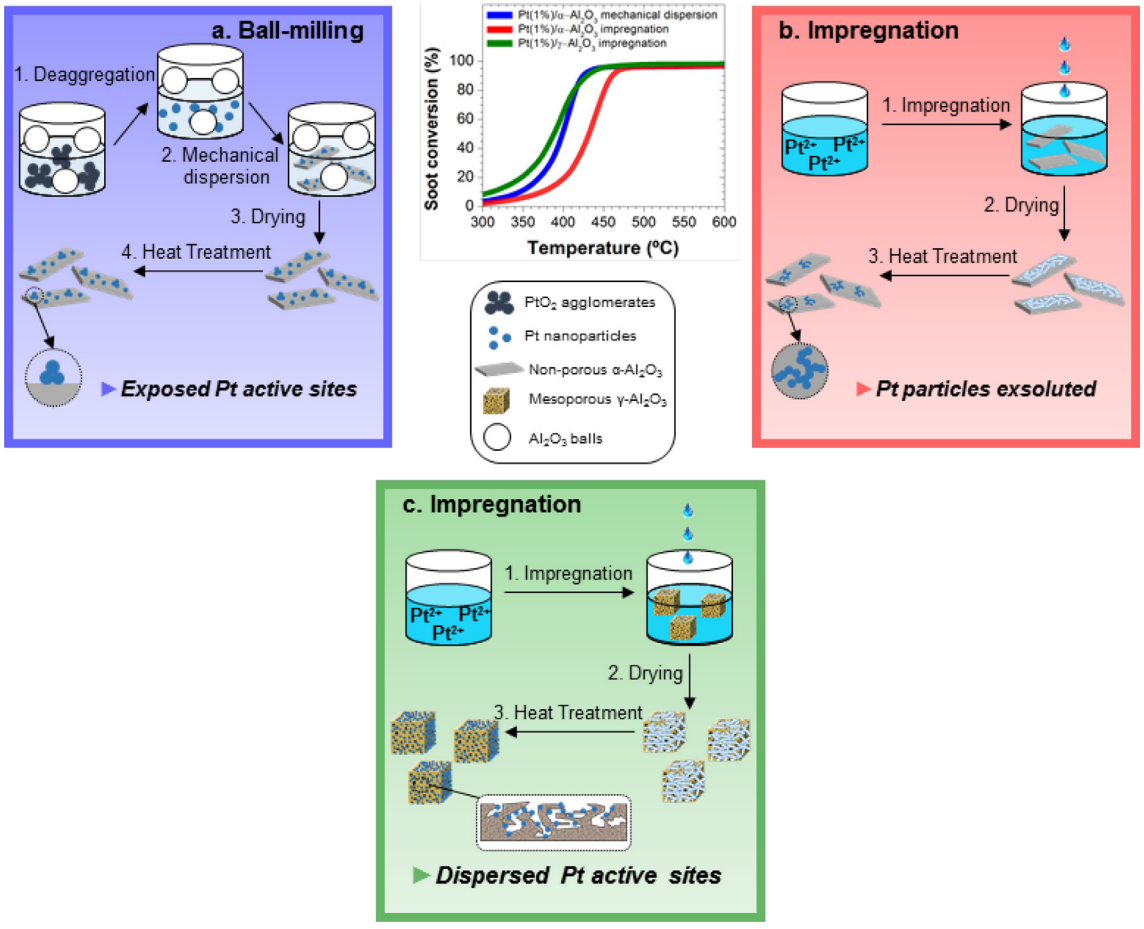


**Fig. 3.** Schematic representation of the dispersion of Pt particles on the external surface of the $\alpha$-$Al_2O_3$ support (a and b) or the mesopores of the $\gamma$-$Al_2O_3$ support (c) by mechanical dispersion (a) or incipient wetness impregnation (b and c).

microreactors implementation and a considerable reduction in the channel size.

## 4. Conclusions

A hierarchical catalyst, consisting of Pt particles supported on $\alpha$-$Al_2O_3$ microparticles, was successfully synthesized by a mechanical wet dispersion method. The activity per unit mass of the ball-milled Pt/$\alpha$-$Al_2O_3$ catalyst for soot oxidation in the presence of NO is better than that of the impregnated counterpart, similar to that of the reference sample obtained by impregnation of mesoporous alumina, and improved the best results reported in the state-of-the-art literature for this composition. The location of rather large Pt particles well anchored at the small but easily accessible alpha-alumina surface seems to favor the reaction, despite the relatively low metal dispersion. A further increase in catalytic activity might be expected if the wet-milling process is optimized, and high stability is predicted according to the properties of the alpha phase of alumina, the metal-support interactions achieved by the ball-milling process, and the reproducibility of results when the sample was reused. Thus, the use of a low-energy simple dispersion method seems to be a promising way to reduce the cost of soot oxidation catalysts and improve their performance. We believe that the general strategy described in this work will open new avenues in developing novel catalysts with enhanced properties for many catalytic reactions.

## Declaration of Competing Interest

We wish to confirm that there are no known conflicts of interest associated with this publication and there has been no significant financial support for this work that could have influenced its outcome.

## Acknowledgments

The authors thank the funding bodies of the projects NANOMIND CSIC201560E068 and MAT2017-86450-C4-1-R. C.M. Alvarez-Docio is also thankful for a FPI grant BES-2014-069779, which is co-financed by FEDER funds. F. Rubio-Marcos is indebted to MINECO for a 'Ramon y Cajal' contract (ref: RyC-2015-18626), which is co-financed by the European Social Fund. F.R-M also acknowledges support from Leonardo Grant for Researchers and Cultural Creators (2018), BBVA Foundation.

## Appendix A. Supplementary data

Supplementary data to this article can be found online at https://doi.org/10.1016/j.catcom.2020.105999.

## References

[1] R.J. White, R. Luque, V.L. Budarin, J.H. Clark, D.J. MacQuarrie, Supported metal nanoparticles on porous materials. Methods and applications, Chem. Soc. Rev. 38 (2009) 481–494.
[2] J.R.A. Sietsma, A. Jos van Dillen, P.E. de Jongh, K.P. de Jong, Application of ordered mesoporous materials as model supports to study catalyst preparation by impregnation and drying, Sci. Bases Prep. Heterog. Catal, Elsevier Masson SAS, Amsterdam, 2006, pp. 95–102.
[3] F. Liao, T.W.B. Lo, S.C.E. Tsang, Recent developments in palladium-based bimetallic catalysts, ChemCatChem. 7 (2015) 1998–2014.
[4] M. Komiyama, Design and preparation of impregnated catalysts, Catal. Rev. Sci. Eng. 27 (1985) 341–372.

[5] A. Lekhal, B.J. Glasser, J.G. Khinast, Impact of drying on the catalyst profile in supported impregnation catalysts, Chem. Eng. Sci. 56 (2001) 4473–4487.
[6] K. Ralphs, C. Hardacre, S.L. James, Application of heterogeneous catalysts prepared by mechanochemical synthesis, Chem. Soc. Rev. 42 (2013) 7701–7718.
[7] C. Borchers, M.L. Martin, G.A. Vorobjeva, O.S. Morozova, A.A. Firsova, A.V. Leonov, E.Z. Kurmaev, A.I. Kukharenko, I.S. Zhidkov, S.O. Cholakh, Cu–$CeO_2$ nanocomposites: Mechanochemical synthesis, physico-chemical properties, CO-PROX activity, J. Nanopart. Res. 18 (2016) 344.
[8] C. Tang, B. Sun, J. Sun, X. Hong, Y. Deng, F. Gao, L. Dong, Solid state preparation of NiO-$CeO_2$ catalyst for NO reduction, Catal. Today 281 (2017) 575–582.
[9] J. Oi-Uchisawa, S. Wang, T. Nanba, A. Ohi, A. Obuchi, Improvement of Pt catalyst for soot oxidation using mixed oxide as a support, Appl. Catal. B Environ. 44 (2003) 207–215.
[10] J. Lee, E.J. Jang, J.H. Kwak, Effect of number and properties of specific sites on alumina surfaces for Pt-$Al_2O_3$ catalysts, Appl. Catal. A Gen. 569 (2019) 8–19.
[11] C.M. Álvarez-Docio, R. Portela, J.J. Reinosa, F. Rubio-Marcos, C. Granados-Miralles, L. Pascual, J.F. Fernández, Pt-free $CoAl_2O_4$ catalyst for soot combustion with $NO_x$/$O_2$, Appl. Catal. A Gen. 591 (2020) 117404.
[12] F. Rubio-Marcos, V. Calvino-Casilda, M.A. Bañares, J.F. Fernandez, Novel hierarchical $Co_3O_4$/ZnO mixtures by dry nanodispersion and their catalytic application in the carbonylation of glycerol, J. Catal. 275 (2010) 288–293.
[13] M. Danielis, S. Colussi, C. de Leitenburg, L. Soler, J. Llorca, A. Trovarelli, Outstanding methane oxidation performance of palladium-embedded ceria catalysts prepared by a one-step dry ball-milling method, Angew. Chem. Int. Ed. 57 (2018) 10212–10216.
[14] A. Tanimu, S. Jaenicke, K. Alhooshani, Heterogeneous catalysis in continuous flow microreactors: a review of methods and applications, Chem. Eng. J. 327 (2017) 792–821.
[15] A. Piras, S. Colussi, A. Trovarelli, V. Sergo, J. Llorca, R. Psaro, L. Sordelli, Structural and morphological investigation of ceria-promoted $Al_2O_3$ under severe reducing/oxidizing conditions, J. Phys. Chem. B 109 (2005) 11110–11118.
[16] A. Martínez-Arias, M. Fernández-García, L.N. Salamanca, R.X. Valenzuela, J.C. Conesa, J. Soria, Structural and redox properties of ceria in alumina-supported ceria catalyst supports, J. Phys. Chem. B 104 (2000) 4038–4046.
[17] M.R. Gao, Z.Y. Lin, J. Jiang, C.H. Cui, Y.R. Zheng, S.H. Yu, Completely green synthesis of colloid Adams' catalyst α-$PtO_2$ nanocrystals and derivative Pt nanocrystals with high activity and stability for oxygen reduction, Chem. A Eur. J. 18 (2012) 8423–8429.
[18] R.W. McCabe, P.J. Mitchell, Reactions of ethanol and acetaldehyde over noble metal and metal oxide catalysts, Ind. Eng. Chem. Prod. Res. Dev. 23 (1984) 196–202.
[19] R.D. Gonzalez, N. Masatoshi, Oxidation of ethanol on silica supported noble metal and bimetallic catalysts, Appl. Catal. 18 (1985) 57–70.
[20] L.M. Petkovic, S.N. Rashkeev, D.M. Ginosar, Ethanol oxidation on metal oxide-supported platinum catalysts, Catal. Today 147 (2009) 107–114.
[21] T.H. Fleisch, G.J. Mains, Photoreduction and reoxidation of platinum oxide and palladium oxide surfaces, J. Phys. Chem. 90 (1986) 5317–5320.
[22] A. Dicko, X.M. Song, A. Adnot, A. Sayari, Characterization of platinum on sulfated zirconia catalysts by temperature programmed reduction, J. Catal. 150 (1994) 254–261.
[23] F.A. De Bruijn, G.B. Marin, J.W. Niemantsverdriet, W.H.M. Visscher, J.A.R. Van Veen, Characterization of graphite-supported platinum catalysts by electrochemical methods and XPS, Surf. Interface Anal. 19 (1992) 537–542.
[24] M. Casapu, J.D. Grunwaldt, M. Maciejewski, F. Krumeich, A. Baiker, M. Wittrock, S. Eckhoff, Comparative study of structural properties and NOx storage-reduction behavior of Pt/Ba/$CeO_2$ and Pt/Ba/$Al_2O_3$, Appl. Catal. B Environ. 78 (2008) 288–300.
[25] Z. Lodziana, J.K. Nørskov, Adsorption of Cu and Pd on α-$Al_2O_3$ (0001) surfaces with different stoichiometries, J. Chem. Phys. 115 (2001) 11261–11267.
[26] I. Lorite, L. Pérez, J.J. Romero, J.F. Fernandez, Effect of the dry nanodispersion procedure in the magnetic order of the $Co_3O_4$ surface, Ceram. Int. 39 (2013) 4377–4381.
[27] I. Lorite, M.S. Martín-González, J.J. Romero, M.A. García, J.L.G. Fierro, J.F. Fernández, Electrostatic charge dependence on surface hydroxylation for different $Al_2O_3$ powders, Ceram. Int. 38 (2012) 1427–1434.
[28] S. Liu, X. Wu, D. Weng, R. Ran, $NO_x$-assisted soot oxidation on Pt-mg/$Al_2O_3$ catalysts: magnesium precursor, Pt particle size, and Pt-mg interaction, Ind. Eng. Chem. Res. 51 (2012) 2271–2279.
[29] Y. Gao, W. Yang, X. Wu, S. Liu, D. Weng, R. Ran, Controllable synthesis of supported platinum catalysts: acidic support effect and soot oxidation catalysis, Catal. Sci. Technol. 7 (2017) 3268–3274.
[30] J. Giménez-Mañogil, A. García-García, Opportunities for ceria-based mixed oxides versus commercial platinum-based catalysts in the soot combustion reaction. Mechanistic implications, Fuel Process. Technol. 129 (2015) 227–235.
[31] C.M. Kalamaras, S. Americanou, A.M. Efstathiou, "Redox" vs "associative formate with -OH group regeneration" WGS reaction mechanism on Pt/$CeO_2$: effect of platinum particle size, J. Catal. 279 (2011) 287–300.
[32] A. Boubnov, S. Dahl, E. Johnson, A.P. Molina, S.B. Simonsen, F.M. Cano, S. Helveg, L.J. Lemus-Yegres, J.D. Grunwaldt, Structure-activity relationships of Pt/$Al_2O_3$ catalysts for CO and NO oxidation at diesel exhaust conditions, Appl. Catal. B Environ. 126 (2012) 315–325.
[33] S.S. Mulla, N. Chen, L. Cumaranatunge, G.E. Blau, D.Y. Zemlyanov, W.N. Delgass, W.S. Epling, F.H. Ribeiro, Reaction of NO and $O_2$ to $NO_2$ on Pt: kinetics and catalyst deactivation, J. Catal. 241 (2006) 389–399.
[34] C.K. Narula, L.F. Allard, G.M. Stocks, M. Moses-Debusk, Remarkable NO oxidation on single supported platinum atoms, Sci. Rep. 4 (2014) 1–6.
[35] B.M. Weiss, E. Iglesia, NO oxidation catalysis on Pt clusters: elementary steps, structural requirements, and synergistic effects of $NO_2$ adsorption sites, J. Phys. Chem. C 113 (2009) 13331–13340.